

Future Impact of Differential Interbasin Ocean Warming on Atlantic Hurricanes

SANG-KI LEE AND DAVID B. ENFIELD

Cooperative Institute for Marine and Atmospheric Studies, University of Miami, and NOAA/Atlantic Oceanographic and Meteorological Laboratory, Miami, Florida

CHUNZAI WANG

NOAA/Atlantic Oceanographic and Meteorological Laboratory, Miami, Florida

(Manuscript received 4 June 2010, in final form 1 October 2010)

ABSTRACT

Global climate model simulations forced by future greenhouse warming project that the tropical North Atlantic (TNA) warms at a slower rate than the tropical Indo-Pacific in the twenty-first century, consistent with their projections of a weakened Atlantic thermohaline circulation. Here, an atmospheric general circulation model is used to advance a consistent physical rationale that the suppressed warming of the TNA increases the vertical wind shear and static stability aloft in the main development region (MDR) for Atlantic hurricanes, and thus decreases overall Atlantic hurricane activity in the twenty-first century. A carefully designed suite of model experiments illustrates that the preferential warming of the tropical Indo-Pacific induces a global average warming of the tropical troposphere, via a tropical teleconnection mechanism, and thus increases atmospheric static stability and decreases convection over the suppressed warming region of the TNA. The anomalous diabatic cooling, in turn, forces the formation of a stationary baroclinic Rossby wave northwest of the forcing region, consistent with Gill's simple model of tropical atmospheric circulations, in such a way as to induce a secular increase of the MDR vertical wind shear. However, a further analysis indicates that the net effect of future greenhouse warming on the MDR vertical wind shear is less than the observed multidecadal swing of the MDR vertical wind shear in the twentieth century. Thus, it is likely that the Atlantic multidecadal oscillation will still play a decisive role over the greenhouse warming in the fate of Atlantic hurricane activity throughout the twenty-first century under the assumption that the twenty-first-century changes in interbasin SST difference, projected by the global climate model simulations, are accurate.

1. Introduction

Observations during the satellite era indicate that a 0.5°C increase of North Atlantic sea surface temperature (SST) in the Atlantic hurricane main development region (MDR; 10°–20°N, 85°–15°W) is associated with about a 40% increase in Atlantic hurricane frequency (Saunders and Lea 2008). According to the externally forced model simulations for the twenty-first century used in the Intergovernmental Panel for Climate Change's Fourth Assessment Report (IPCC AR4), the MDR SST may increase by about 2°C or more between 2000 and 2100 because of anthropogenic global warming (AGW). This is alarming given that the MDR SST has never reached such an extremity since reliable and widespread instrumental

measurements became available in the late 1800s. At issue is whether we are entering a new era of much elevated hurricane activity because of the rising global SST.

In the North Atlantic basin, the most critical environmental factors for hurricane intensification are the MDR vertical wind shear (VWS), which impedes the efficient development of organized convection to increasing heights as the storm intensity increases, and the MDR convective instability of the troposphere (Emanuel 1994). Thus, both the MDR VWS and convective instability are useful and widely used proxies for overall Atlantic hurricane activity. In this study, the MDR convective precipitation rate (CPR) is used to represent the MDR convective instability.

Figure 1 shows the 7-yr running-averaged MDR SST anomaly (Fig. 1a), VWS (200 minus 850 mb) anomaly (Fig. 1b), and CPR anomaly (Fig. 1c) for the period 1900–2100 obtained from the ensemble average of 21 IPCC

Corresponding author address: Dr. Sang-Ki Lee, NOAA/AOML, 4301 Rickenbacker Causeway, Miami, FL 33149.
E-mail: sang-ki.lee@noaa.gov

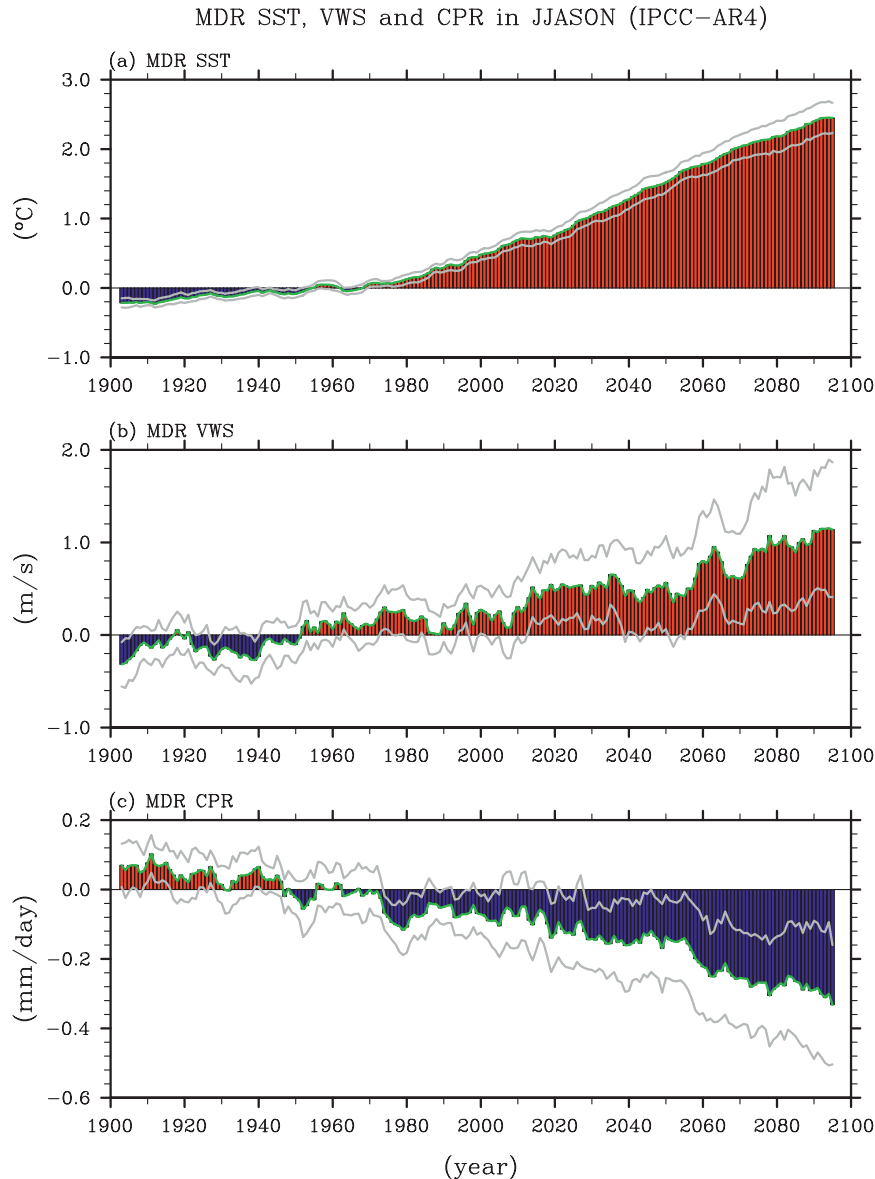


FIG. 1. A 7-yr running mean (a) SST anomaly, (b) VWS (200 minus 850 mb) anomaly, and (c) CPR anomaly averaged in the MDR (10° – 20° N, 85° – 15° W) for the period 1900–2100 obtained from the ensemble average of 21 IPCC AR4 climate model simulations under the 20C3M (1900–99) and A1B (2000–2100) scenarios. The period 1900–99 is used as the baseline for computing the anomalies. Gray lines represent 95% significance, which is computed based on a bootstrap technique.

AR4 climate model simulations under the Twentieth-Century Climate in Coupled Model (20C3M; 1900–99) and A1B (2000–2100) scenarios. The MDR SST increases monotonically by more than 2.5°C between 1900 and 2100. The MDR VWS is characterized by an overall increase with relatively large amplitude of multidecadal variation in the twentieth and twenty-first centuries, whereas the MDR convective instability is significantly reduced between 1900 and 2100. Both the increased

MDR VWS and decreased MDR convective instability suggest that Atlantic cyclone activity could be reduced in the twenty-first century despite an increase in the MDR SST by 2.5°C (Vecchi and Soden 2007c). Note that Wang and Lee (2008) also reported a similar upward trend in the observed MDR VWS during a relatively short period of 1949–2006.

The upward (downward) trend in MDR VWS (convective instability) and the simultaneous increase in MDR

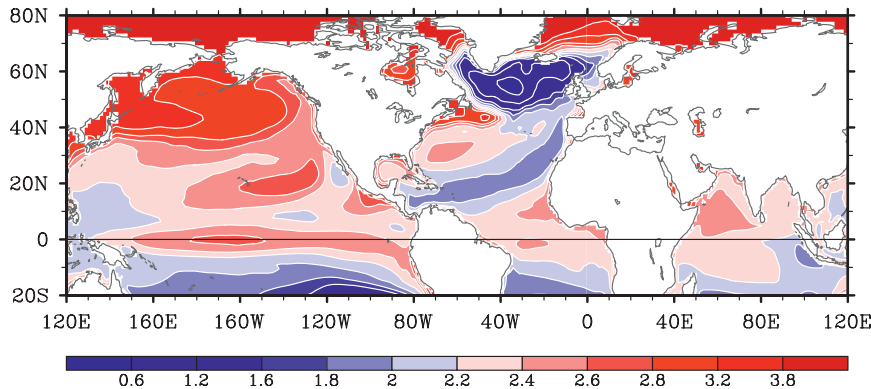


FIG. 2. Linear trend of SST [$^{\circ}\text{C} (100 \text{ yr})^{-1}$] in JJASON during the 2000–2100 periods computed from the ensemble average of 21 IPCC AR4 climate simulations under the A1B scenario.

SST are apparently inconsistent with recent research, which shows, based on theory, observations and models, that a warm tropical North Atlantic (TNA) SST is associated with an increase in the MDR convective instability, decreases in the MDR subsidence and sea level pressure, and a weakened tropical upper-tropospheric trough circulation, and thus reduces the MDR VWS (Knaff 1997; Knight et al. 2006; Wang et al. 2006; Zhang and Delworth 2006; Vimont and Kossin 2007; Kossin and Vimont 2007). Therefore, it appears that using the observed correlation in the twentieth century between the MDR SST and MDR VWS (or convective instability) for projecting Atlantic hurricane activity of the twenty-first century could be misleading.

A newly emerging hypothesis provides us with some insights as to why this may be the case (Latif et al. 2007; Swanson 2008; Vecchi and Soden 2007a; Wang and Lee 2008). The main argument of the hypothesis is that Atlantic hurricanes do not respond to the absolute SST of the MDR but to the SST difference between the MDR and the other tropical ocean basins (hereafter referred to as *differential interbasin ocean warming hypothesis*). Therefore, it argues that an important and relevant question is whether and how the MDR is warming at a different rate from the tropical Indo-Pacific (TIP) under the AGW scenarios.

As shown in Fig. 2, the IPCC AR4 climate model simulations project that the MDR indeed warms at a slower rate than the tropical Indo-Pacific in the twenty-first century, which is consistent with the projections of a weakened Atlantic thermohaline circulation given an apparent coherent relation between the Atlantic thermohaline circulation and the TNA SST (Zhang and Delworth 2005; Timmermann et al. 2007; Zhang 2007; Chiang et al. 2008). It is also noticed that the equatorial Pacific, which is known to be an important region to remotely influence the MDR VWS (Gray 1984; Goldenberg and Shapiro 1996; Latif

et al. 2007), warms at a faster rate than the MDR, consistent with the IPCC AR4 climate model projections of the weakening Pacific Walker circulation (Vecchi and Soden 2007b; DiNezio et al. 2009). Whatever the mechanism that causes the differential interbasin ocean warming in the IPCC AR4 climate model simulations, at issue is whether the reduced warming of the MDR is the real cause of the projected secular increase (decrease) of the MDR VWS (convective instability) in the twenty-first century.

To address this important issue, we here explore the atmospheric dynamics that provide physical basis for the differential interbasin ocean warming hypothesis by performing a set of climate model experiments using an atmospheric general circulation model. Toward the end, we attempt to explain the IPCC AR4 projected secular increase (decrease) of the MDR VWS (convective instability) in the twenty-first century by using the causal relationship of the interbasin SST difference with the MDR VWS (convective instability).

2. Model experiments

The National Center for Atmospheric Research (NCAR) Community Atmospheric Model, version 3 (CAM3) is used as a primary tool for this study. The CAM3 is a global spectral model with a triangular spectral truncation of the spherical harmonics at zonal wavenumber 85 (T85) and with 26 hybrid sigma-pressure layers. The CAM3 is the atmospheric component of Community Climate System Model, version 3 (CCSM3), which is one of the climate models used in IPCC AR4. Model experiments are performed by prescribing various composites of global SST and sea ice fraction, taken from the ensemble average of 11 IPCC AR4 climate model simulations. The 11 IPCC AR4 model simulations are selected because they show a consistent upward trend of MDR VWS in the twenty-first century under the A1B scenario.

TABLE 1. Global SST and sea ice fraction prescribed in the four CAM3 experiments are obtained from the ensemble average of 11 IPCC AR4 climate simulations for the twenty-first century under the A1B scenario for the periods described in this table. Also shown in this table are the TIP and MDR SST increases in each experiment in reference to the control experiment. CO₂ level specified for the three experiments is also summarized in this table. Refer to text for more detail.

Expt	TIP SST increase	MDR SST increase	Global SST	Sea ice fraction	CO ₂ level (ppm)
EXP_CTRL	—	—	2001–20	2001–20	380
EXP_GLBW	2.05	1.64	2081–2100	2081–2100	675
EXP_WTNA	2.05	2.05	2081–2100	2081–2100	675

We have performed three sets of model experiments, as summarized in Table 1. In the control experiment (EXP_CTRL), the global SSTs and sea ice fractions are prescribed with 12 monthly climatological values taken from the ensemble average of the 11 IPCC AR4 climate simulations for the period 2001–20. The CO₂ level is fixed at 380 ppm, which is the averaged CO₂ level for 2001–20 under the A1B scenario. Similarly, in the global ocean warming experiment (EXP_GLBW), the global SSTs and sea ice fractions are prescribed with 12 monthly climatological values taken from the ensemble average of the 11 IPCC AR4 climate simulations for the period 2081–2100. The CO₂ level is fixed at 675 ppm, which is the averaged CO₂ level for 2081–2100 under the A1B scenario. Figure 3a shows the SST difference between EXP_GLBW and EXP_CTRL during the Atlantic hurricane season of June–November (JJASON). Comparing EXP_GLBW with EXP_CTRL, the MDR SST is warmer by 1.64°C, while the TIP (from the east coast of Africa to the west coast of the Americas, and from the equator to 30°N) SST is warmer by 2.05°C, indicating a 0.41°C (80 yr)⁻¹ of differential warming rate between the two regions. Finally, the warmer TNA experiment (EXP_WTNA) is designed to isolate the impact of the suppressed TNA warming. In this experiment, the global sea ice fractions are taken from the ensemble average of the 11 IPCC AR4 climate simulations for the period 2081–2100, and the CO₂ level is fixed at 675 ppm following the A1B scenario. SSTs in the suppressed warming region of the TNA between the equator and 40°N are increased in such a way that the MDR SST warming is equal to the TIP warming of 2.05°C, whereas the SSTs outside of the suppressed warming region of the TNA are identical to those of EXP_GLBW (see Fig. 3 and Table 1 for more details).

In each model experiment, the model is integrated for 25 yr. The first 10 yr of model output are discarded to exclude any possible transient spinup effects. The remaining

15 yr of model output are averaged to suppress internal atmospheric variability. To isolate the effects of differential interbasin ocean warming associated with AGW, the differences between EXP_GLBW and EXP_CTRL, between EXP_WTNA and EXP_GLBW, and between EXP_WTNA and EXP_CTRL are described and compared with the corresponding ensemble average of the 11 IPCC AR4 climate simulations in the next section.

It is important to keep in mind that EXP_WTNA – EXP_GLBW represents a warmer minus cooler TNA. In the case of EXP_GLBW – EXP_CTRL, many forcing factors are represented, including 1) global ocean warming, 2) increased greenhouse gas, and 3) suppressed warming of the TNA in contrast to the TIP warming. In the next section, it will be demonstrated that factor 3 is the only major factor to influence the MDR VWS and convective instability.

3. Results

Figure 4a shows the VWS difference between the periods 2080–2100 and 2000–20 in JJASON, computed from the ensemble average of the 11 IPCC AR4 climate simulations under the A1B scenario, whereas Figs. 4b and 4c show the VWS difference in JJASON between EXP_GLBW and EXP_CTRL and between EXP_WTNA and EXP_GLBW, respectively. The composite difference in IPCC AR4 model simulations (Fig. 4a) is characterized by an increase in the MDR VWS, particularly over the Caribbean Sea, with an averaged amplitude of about 1.6 m s⁻¹ in the MDR. The global ocean warming minus control run (Fig. 4b) is also characterized by an increased MDR VWS, which is focused over the same region (i.e., the Caribbean Sea) as in the IPCC AR4 composite difference (Fig. 4a) with comparable amplitude. In this case, however, the MDR box-averaged VWS increases only by 0.6 m s⁻¹ because the positive VWS change over the Caribbean Sea does not extend into the eastern TNA. In the warmer TNA minus global ocean warming run (Fig. 4c), the MDR VWS over the Caribbean Sea is substantially weakened as expected from the earlier studies (Knight et al. 2006; Wang et al. 2006; Zhang and Delworth 2006), with about -1.0 m s⁻¹ averaged in the MDR box. This result clearly indicates that the MDR VWS increase in EXP_GLBW – EXP_CTRL could be almost negated if the warming rate of the MDR in the twenty-first century were as large as that of the TIP. The apparent similarity in the spatial pattern and amplitude of the MDR VWS changes between EXP_GLBW and EXP_CTRL (Fig. 4b) and between EXP_WTNA and EXP_GLBW (Fig. 4c) strongly suggests that the main driver for the MDR VWS increase in EXP_GLBW – EXP_CTRL

SST Change in JJASON

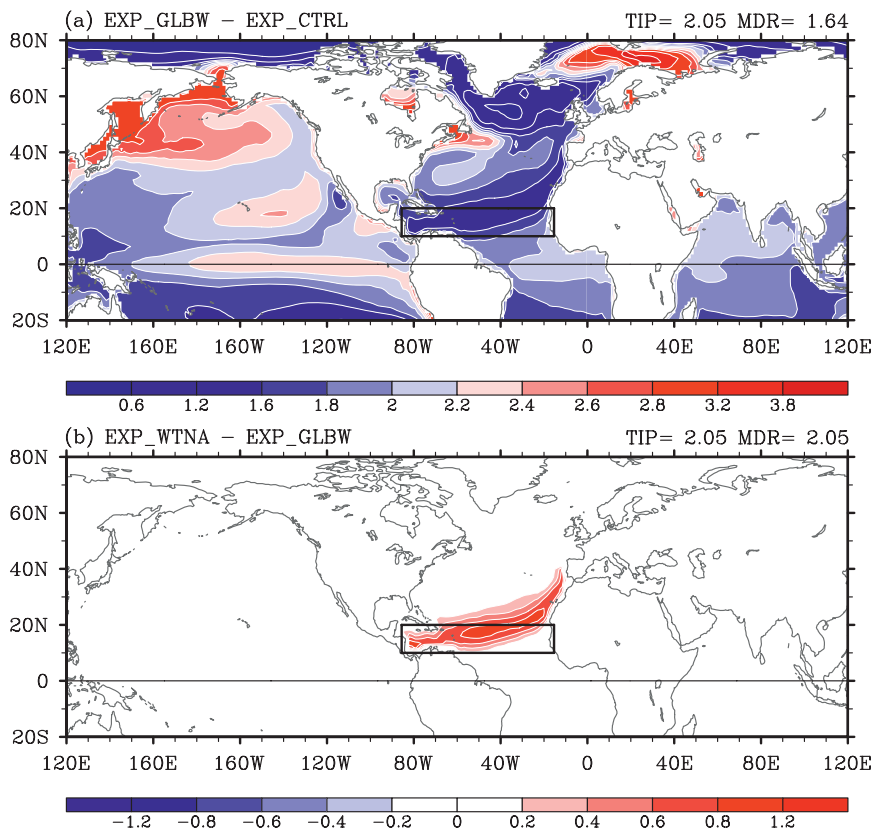


FIG. 3. SST difference ($^{\circ}\text{C}$) in JJASON for (a) EXP_GLBW - EXP_CTRL and (b) EXP_WTNA - EXP_GLBW. The box region indicates the MDR for Atlantic hurricanes (10° - 20°N , 85° - 15°W). The MDR-averaged SST difference between EXP_GLBW and EXP_CTRL is indicated in the upper right corner of (a) along with the SST difference averaged in the TIP (from the east coast of Africa to the west coast of the Americas, and from the equator to 30°N). Similarly, the MDR-averaged SST difference between EXP_WTNA and EXP_CTRL is indicated in the upper right corner of (b) along with the SST difference averaged in the TIP.

is the suppressed warming of the TNA in contrast to the TIP. Thus, the differential interbasin ocean warming response to the AGW explains why a secular increase of MDR SST in the IPCC AR4 model simulations does not necessarily result in a secular decrease in MDR VWS. We will come back to this point in the latter part of this section, where we present a consistent physical rationale that supports the differential interbasin ocean warming hypothesis.

To further understand the atmospheric dynamics associated with the MDR VWS changes shown in Fig. 4, we now examine the horizontal gradient of geopotential thickness between the upper and lower troposphere, which is dynamically related to VWS via the thermal wind relationship. Figure 5a shows the geopotential thickness and VWS (200 minus 850 mb) vector differences in JJASON between the periods 2080-2100 and 2000-20, computed from the ensemble average of the

11 IPCC AR4 climate simulations under the A1B scenario, whereas Figs. 5b and 5c show the geopotential thickness and VWS vector differences in JJASON between EXP_GLBW and EXP_CTRL and between EXP_WTNA and EXP_GLBW, respectively.

The composite difference of the IPCC AR4 climate model simulations (Fig. 5a) is clearly characterized by a region of minimal thickness and cyclonic vertical shear straddling the eastern North Pacific, the Central American cordillera, and the Gulf of Mexico. The global ocean warming minus control run (Fig. 5b) also shows a similar pattern of the geopotential thickness and VWS vector differences; although in this case, the Atlantic side of the cyclonic gyre is somewhat separated from the Pacific side by the Sierra Madre and Rocky Mountains and much stronger than the Pacific side. (The discrepancies between Figs. 5a and 5b, which are particularly large over the eastern TNA and North Africa, can be attributed to

Vertical Wind Shear Change in JJASON

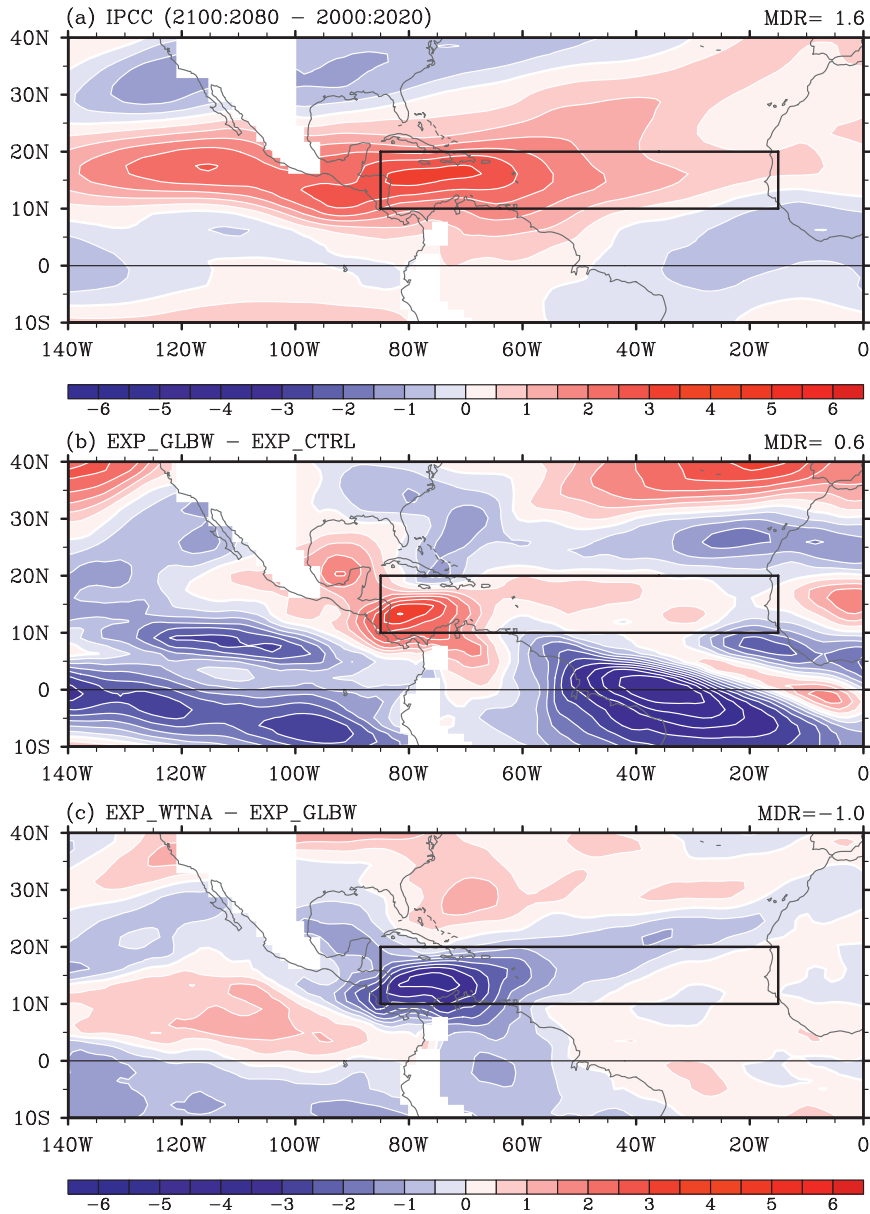


FIG. 4. (a) VWS (200 minus 850 mb) difference in JJASON between the periods 2080–2100 and 2000–20 computed from the ensemble average of 11 IPCC AR4 climate simulations under the A1B scenario. The VWS difference in JJASON for (b) EXP_GLBW – EXP_CTRL and (c) EXP_WTNA – EXP_GLBW. White areas are mountain regions without 850-mb data. The box region indicates the MDR for Atlantic hurricanes.

model-to-model variation in response to external SST forcings.) The mean atmospheric circulation in boreal summer over the TNA features the easterly trade winds in the lower troposphere and the westerly winds in the upper troposphere. Thus, the wind patterns associated with the baroclinic cyclone strengthen both the lower-tropospheric easterly winds and the upper-tropospheric

westerly winds over the Caribbean Sea, resulting in an increase of the MDR VWS.

In the case of the warmer TNA minus global ocean warming run (Fig. 5c), an intense baroclinic anticyclone is formed in a broad region extending from the eastern North Pacific to the western TNA. The wind patterns associated with the baroclinic anticyclone decrease the

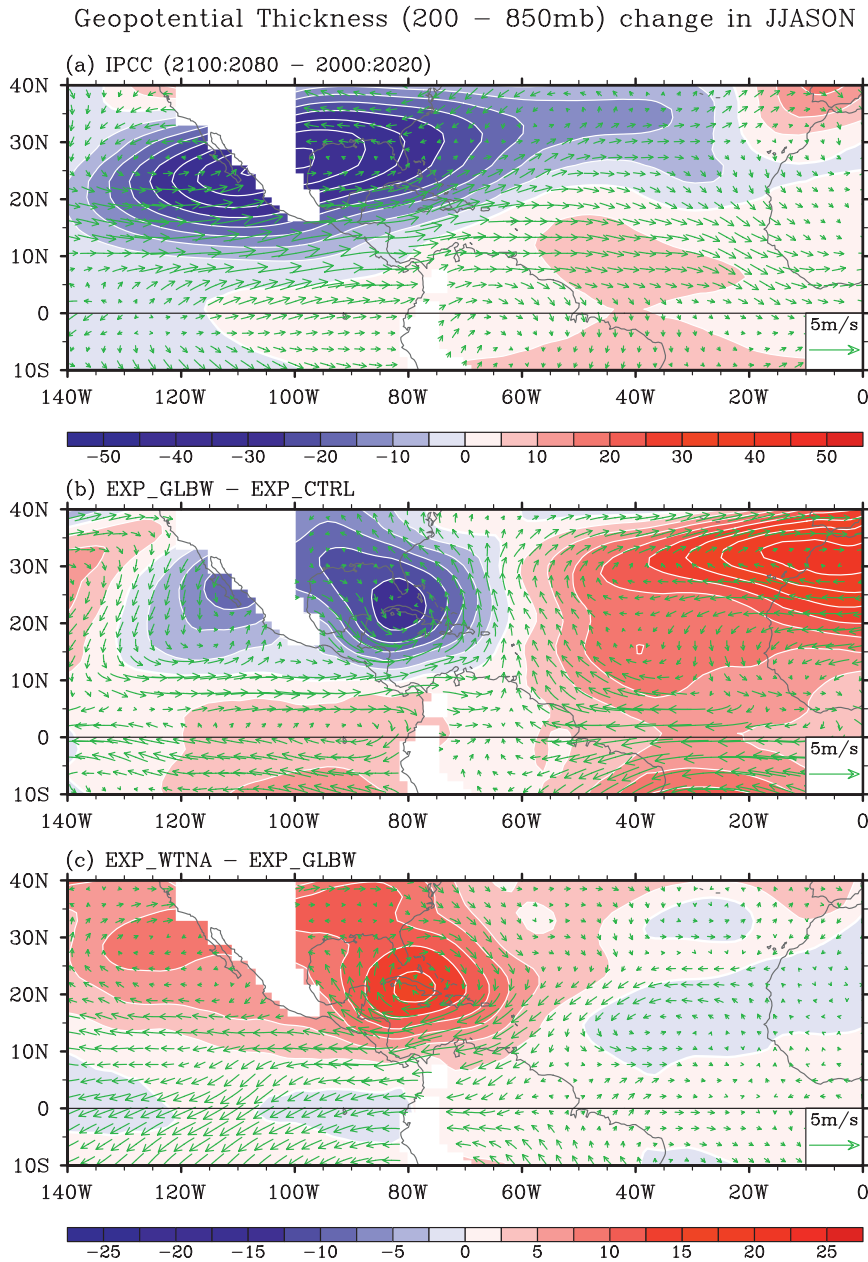


FIG. 5. (a) Geopotential thickness and VWS vector (200 minus 850 mb) differences in JJASON between the periods 2080–2100 and 2000–20 computed from the ensemble average of 11 IPCC AR4 climate simulations under the A1B scenario. Geopotential thickness and VWS vector differences in JJASON for (b) EXP_GLBW – EXP_CTRL and (c) EXP_WTNA – EXP_GLBW. White areas are mountain regions without 850-mb data. Dynamic responses of the atmosphere to AGW are most prominent over high latitudes around 50°–60°N, with a significant amplitude in zonally averaged components (not shown). Since the main interest is tropical atmospheric dynamics around the MDR, the zonal mean components of geopotential thickness difference are removed. Note that the zonal means are not removed in VWS difference.

MDR VWS. The baroclinic atmospheric response in this case is largely consistent with the Gill model's solution to a diabatic-heating in the TNA associated with the prescribed SST pattern (Fig. 3b), and thus can be referred to as a heat-induced stationary baroclinic Rossby wave (Gill 1980). It is immediately noticed that the baroclinic cyclone in EXP_GLBW – EXP_CTRL (Fig. 5b) is almost a mirror image to the baroclinic anticyclone in EXP_WTNA – EXP_GLBW (Fig. 5c), and thus consistent with the Gill model's solution to a diabatic *cooling* in the TNA. However, note that the prescribed MDR SST is warmer in EXP_GLBW than in EXP_CTRL by 1.64°C. Apparently, the positive MDR SST forcing in EXP_GLBW – EXP_CTRL is in contradiction with a diabatic cooling in the TNA.

To explain this conundrum, we present the following physical rationale. Even though the TNA SST is warmer in EXP_GLBW than in EXP_CTRL, the overlying atmosphere is also warmed because of the global average tropospheric warming of the tropics, which is largely induced by the increased SSTs in the TIP. In other words, the tropical troposphere tends to respond to surface heating in a zonally symmetric fashion, such that the temperature difference between the troposphere and the differentially heated surface layer (i.e., the atmospheric static instability) will be greater in the TIP and less in the TNA, thus affecting the thickness field as shown in Fig. 5b. Therefore, in this sense, the suppressed warming of the TNA increases the atmospheric static stability and decreases the convection aloft, and thus evokes a Gill response consistent with local diabatic cooling.

To substantiate this physical explanation, the MDR-averaged atmospheric heating rate (longwave and convective) and pressure velocity from the three CAM3 experiments are plotted in Fig. 6. Note that the longwave cooling is increased in both EXP_GLBW and EXP_WTNA from EXP_CTRL, suggesting that the differential interbasin ocean warming has much smaller impact on radiative cooling of the troposphere aloft of the MDR in comparison to other AGW impacts—a slightly reduced midtropospheric longwave cooling in EXP_WTNA from EXP_GLBW can be attributed to the increased MDR convection, as suggested in Knaff (1997). On the other hand, the convective heating is much reduced in EXP_GLBW – EXP_CTRL but not in EXP_WTNA – EXP_CTRL. Consistently, EXP_GLBW – EXP_CTRL is characterized by an enhanced subsidence throughout the entire troposphere aloft the MDR, whereas EXP_WTNA – EXP_CTRL is characterized with a weakly enhanced subsidence only in the upper troposphere, possibly associated with the increased radiative cooling in the upper troposphere. The convective precipitation changes shown

in Fig. 7 also clearly support the physical rationale explained here.

A similar argument has been used to explain the observed global tropospheric warming in the tropics associated with El Niño (e.g., Chiang and Sobel 2002). The physical background for this argument is that atmospheric Kelvin waves tend to redistribute temperature anomalies originating at one particular longitude band over the global tropical strip, which is a very efficient mechanism for tropical teleconnections. Note that the physical rationale provided here is also consistent with Xie et al. (2010), who showed the importance of regional differences in SST warming for tropical convection.

In summary, our model experiments clearly demonstrate that the main driver for the increased MDR VWS and decreased MDR convective instability in the IPCC AR4 climate model simulations for the twenty-first century is the formation of a baroclinic cyclone to the northwest of the MDR, which is a Gill response to a diabatic cooling associated with the suppressed warming of the TNA in contrast to the TIP.

4. Discussion

We now have a consistent physical rationale for expecting a significant relationship between a differential interbasin ocean warming and the MDR VWS and convective instability in the North Atlantic sector. Naturally, the next question is how well this relationship explains the secular increase (decrease) of the MDR VWS (convective instability) within the twenty-first century projected by the IPCC AR4 climate model simulations.

Figure 8a shows the time series of reconstructed MDR VWS in JJASON for the period 1900–2100 based on a multiple regression of the MDR VWS onto the MDR SST and TIP SST from the ensemble average of the 21 IPCC AR4 climate model simulations under the 20C3M and A1B scenarios. The MDR CPR is also reconstructed using the MDR SST and the TIP SST as the predictors for a multiple regression, as shown in Fig. 8b.

A close inspection of Figs. 1 and 8 suggests that the original time series and the least squares fits share similar long-term signals and overall trend throughout 1900–2100. The least squares equations used for reconstructing MDR VWS and CPR are given by $\text{MDR VWS} = -2.7 \times \text{MDR SST} + 3.0 \times \text{TIP SST}$ and $\text{MDR CPR} = 0.9 \times \text{MDR SST} - 1.0 \times \text{TIP SST}$, respectively. These equations confirm that a uniform warming of the MDR SST and TIP SST has little impact on the MDR VWS and convective instability, which are the two most critical environmental factors for Atlantic hurricane activity, and that the interbasin SST difference is the most important indicator and predictor of Atlantic hurricane activity for

MDR-Averaged Heating Rate and Pressure Velocity in JJASON

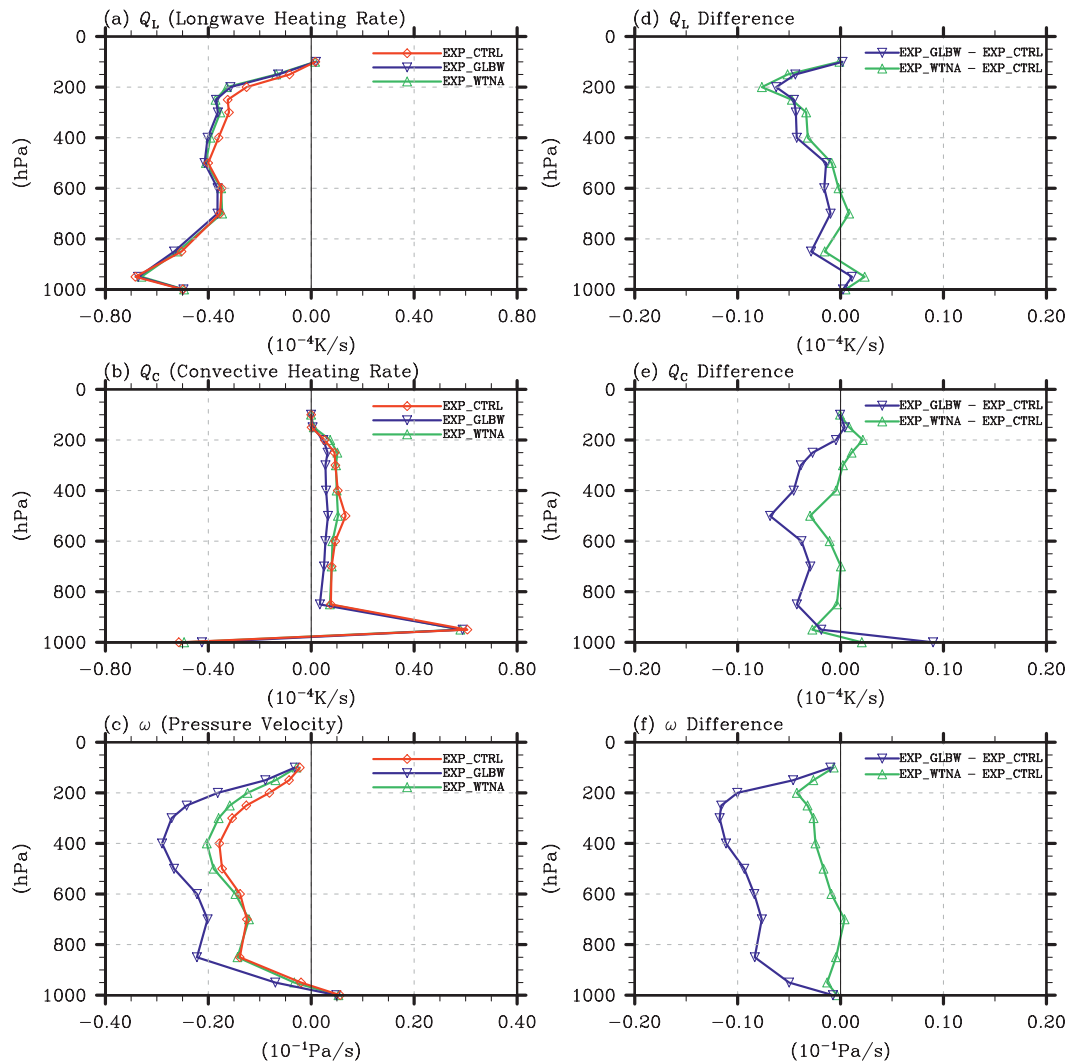


FIG. 6. MDR-averaged (a) longwave (Q_L) and (b) convective (Q_C) heating rates and (c) pressure velocity (ω) in JJASON computed from EXP_CTRL, EXP_GLBW, and EXP_WTNA. Changes of (d) Q_L , (e) Q_C , and (f) ω in EXP_GLBW and EXP_WTNA in reference to EXP_CTRL. The pressure velocity is positive upward.

both the twentieth and twenty-first centuries, consistent with Vecchi et al. (2008). Multiple linear regressions similar to Fig. 8 are also performed for 18 IPCC AR4 model simulations, individually. With an exception of only 1 model simulation, the 7-yr running-averaged MDR VWS is negatively correlated with the 7-yr running-averaged MDR SST and positively correlated with the 7-yr running-averaged TIP SST, confirming the robust relationship between the interbasin SST difference and the MDR VWS.

At the multidecadal or longer time scales, the observed MDR VWS during 1949–2006 changes by up to 4.0 m s^{-1} (Wang et al. 2008), whereas the ensemble average of IPCC

AR4 model simulations projects that the MDR VWS increases by about 1.0 m s^{-1} in the late twenty-first century (Fig. 1b). Therefore, if the twenty-first-century changes in interbasin SST difference projected by the IPCC AR4 model simulations are accurate, then the net effect of AGW on the MDR VWS is less than the observed multidecadal swing in the twentieth century associated with the Atlantic multidecadal oscillation (AMO). Note that the IPCC AR4 model simulations underestimate the multidecadal swing of the observed MDR VWS in the twentieth century because the internally generated multidecadal signals are canceled out after applying the ensemble mean (Knight 2009; Ting et al. 2009).

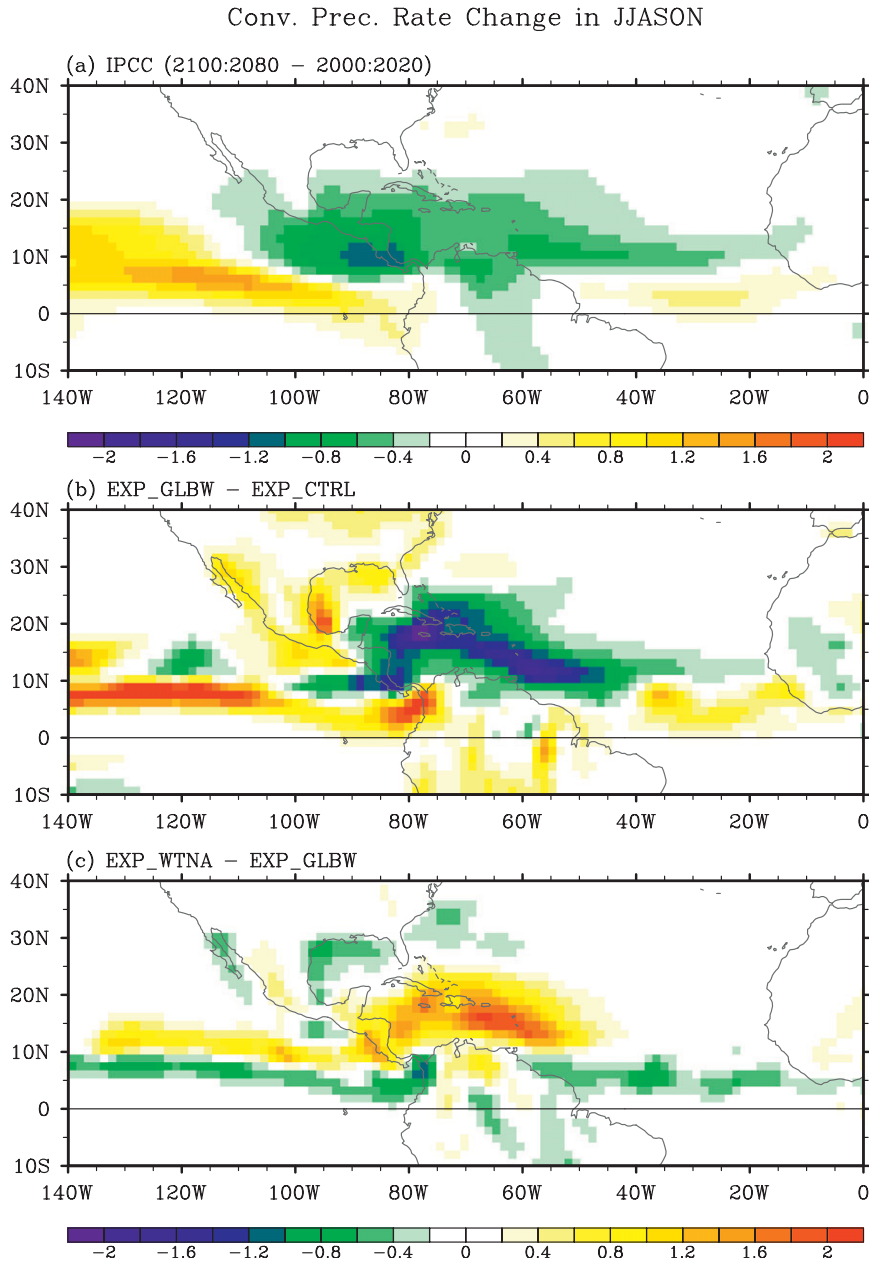


FIG. 7. (a) CPR difference (mm day^{-1}) in JJASON between the periods 2080–2100 and 2000–20 computed from the ensemble average of the 11 IPCC AR4 climate simulations under the A1B scenario. The CPR difference in JJASON for (b) EXP_GLBW – EXP_CTRL and (c) EXP_WTNA – EXP_GLBW.

An important and practical question is why the tropical Indo-Pacific warms faster than the TNA in the IPCC AR4 climate model simulations for the twenty-first century. Given the existing evidence from research that the cold AMO phase occurs in concert with decreases in the Atlantic thermohaline circulation (e.g., Delworth and Mann 2000; Knight et al. 2006), the suppressed warming of the TNA, in reference to the warming in the tropical

Indo-Pacific, is consistent with the IPCC AR4 projection of a significantly weakened Atlantic meridional overturning circulation (AMOC) in the twenty-first century—about 25% weaker in the models that produce a reasonable AMOC in the twentieth century. Apart from the potential contributions of the weakening AMOC, recent studies by Leloup and Clement (2009) and Xie et al. (2010) provide an alternative explanation for the

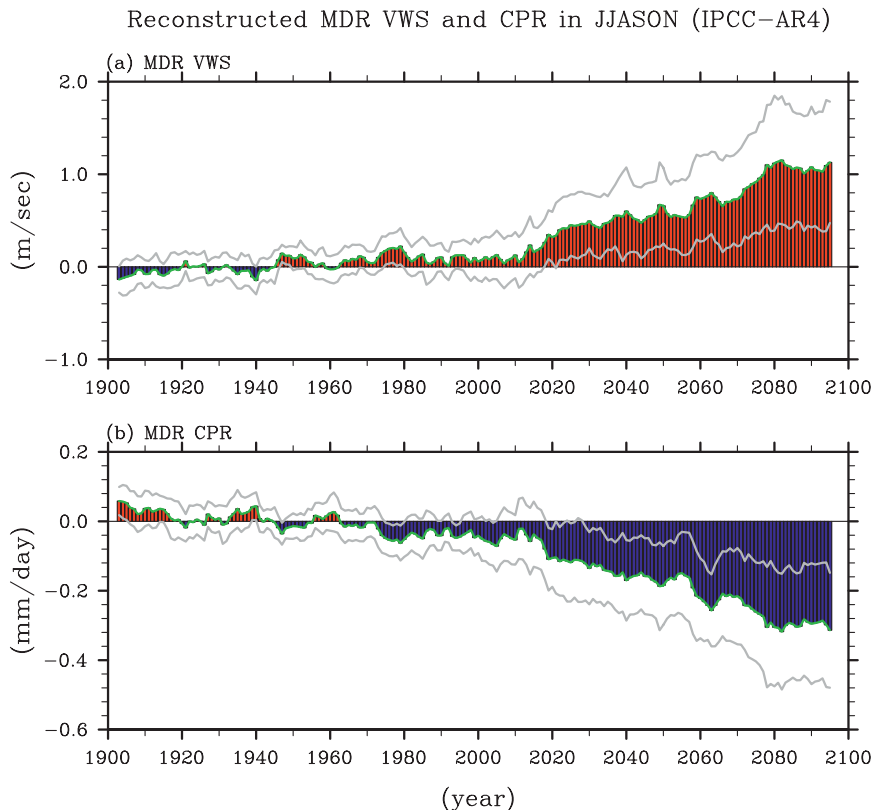


FIG. 8. Times series of reconstructed (a) MDR VWS and (b) CPR in JJASON for the period 1900–2100 based on multiple regressions of the MDR VWS and CPR onto the MDR SST and TIP SST from the ensemble average of 21 IPCC AR4 climate model simulations under the 20C3M and A1B scenarios. A 7-yr running mean is applied to all indices before applying the multiple regressions.

suppressed warming of the TNA. Their main argument is that a uniform increase of SST may result in a greater evaporative cooling response in the region of high mean surface wind speed, such as in the TNA, because the mean surface wind speed serves as the efficiency of evaporative cooling response to external forcing. Further studies are warranted to clarify why the IPCC AR4 climate models project a suppressed warming in the TNA and how reliable that projection is.

In this study, we are mainly concerned with secular changes in the Atlantic hurricane climatology in the twenty-first century using the MDR VWS and CPR from the IPCC AR4 model simulations as the proxies. However, it is also important to understand the changes in the amplitude of short-term variability, especially those associated with El Niño–Southern Oscillation (ENSO; Gray 1984; Goldenberg and Shapiro 1996), the Atlantic warm pool (AWP; Wang et al. 2006; Wang et al. 2008), and the Atlantic meridional mode (AMM; Vimont and Kossin 2007). The IPCC AR4 model simulations project an increase of about 17% in the amplitude of the MDR

VWS at high frequencies (with periods shorter than 7 yr). Further studies are recommended to explore the changes in ENSO, AWP, and AMM, and their relationships with Atlantic hurricane activity in the twenty-first century.

Finally, there remains another crucial question: Is the suppressed warming of the TNA in the IPCC AR4 climate model simulations detectable from observed SST records of the twentieth century? Unfortunately, we do not have a clear answer to this question because it is difficult if not impossible to cleanly separate the secular trend of observed MDR SST from the multidecadal signal of the AMO, which is the dominant mode of SST variability in the North Atlantic (Enfield and Cid-Serrano 2010). For instance, during 1901–2008, the Met Office Hadley Centre Sea Ice and Sea Surface Temperature (HadISST) and extended reconstructed SST, version 3 (ERSST.v3), data give 1.1° and $1.5^{\circ}\text{C} (100\text{ yr})^{-1}$ of secular trends of MDR SST, respectively. During the same period, the secular trends of the TIP SST in the HadISST and ERSST.v3 are 1.0° and $1.4^{\circ}\text{C} (100\text{ yr})^{-1}$, respectively, indicating a preferential warming of the MDR.

However, if a positive AMO phase of 1996–2008 is excluded, the secular trends of MDR SST in the HadISST and ERSST3 drastically drop to 0.8° and $1.2^{\circ}\text{C} (100 \text{ yr})^{-1}$, respectively, whereas the secular trends of the TIP SST in the HadISST and ERSST3 become 0.9° and $1.3^{\circ}\text{C} (100 \text{ yr})^{-1}$, respectively, indicating a suppressed warming of the MDR. An important message here is that the AMO played a decisive role over the AGW in the fate of Atlantic activity in the twentieth century, and it will continue to do so throughout the twenty-first century, assuming that the net effect of AGW on the interbasin SST difference, projected by the IPCC AR4 model simulations, is accurate, and that the AMO is primarily a natural phenomenon, as argued by Enfield and Cid-Serrano (2010).

Acknowledgments. We wish to thank the two anonymous reviewers, Eui-Seok Chung, Anthony Broccoli, Brian Mapes, Ben Kirtman, and Frank Marks for their thoughtful comments and suggestions. This work was supported by a grant from the National Oceanic and Atmospheric Administration's Climate Program Office and by the National Science Foundation (Grant ATM-0850897). The findings and conclusions in this report are those of the authors and do not necessarily represent the views of the funding agencies.

REFERENCES

- Chiang, J. C. H., and A. H. Sobel, 2002: Tropical tropospheric temperature variations caused by ENSO and their influence on the remote tropical climate. *J. Climate*, **15**, 2616–2631.
- , W. Cheng, and C. M. Bitz, 2008: Fast teleconnections to the tropical Atlantic sector from Atlantic thermohaline adjustment. *Geophys. Res. Lett.*, **35**, L07704, doi:10.1029/2008GL033292.
- Delworth, T. L., and M. E. Mann, 2000: Observed and simulated multidecadal variability in the Northern Hemisphere. *Climate Dyn.*, **16**, 661–676.
- DiNezio, P. N., A. C. Clement, G. A. Vecchi, B. J. Soden, B. P. Kirtman, and S.-K. Lee, 2009: Climate response of the equatorial Pacific to global warming. *J. Climate*, **22**, 4873–4892.
- Emanuel, K. A., 1994: *Atmospheric Convection*. Oxford University Press, 580 pp.
- Enfield, D. B., and L. Cid-Serrano, 2010: Secular and multidecadal warmings in the North Atlantic and their relationships with major hurricane activity. *Int. J. Climatol.*, **30**, 174–184, doi:10.1002/joc.1881.
- Gill, A. E., 1980: Some simple solutions for heat-induced tropical circulation. *Quart. J. Roy. Meteor. Soc.*, **106**, 447–462.
- Goldenberg, S. B., and L. J. Shapiro, 1996: Physical mechanisms for the association of El Niño and West African rainfall with Atlantic major hurricane activity. *J. Climate*, **9**, 1169–1187.
- Gray, W. M., 1984: Atlantic seasonal hurricane frequency. Part I: El Niño and 30 mb quasi-biennial oscillation influences. *Mon. Wea. Rev.*, **112**, 1649–1668.
- Knaff, J. A., 1997: Implications of summertime sea level pressure anomalies in the tropical Atlantic region. *J. Climate*, **10**, 789–804.
- Knight, J. R., 2009: The Atlantic multidecadal oscillation inferred from the forced climate response in coupled general circulation models. *J. Climate*, **22**, 1610–1625.
- , C. K. Folland, and A. A. Scaife, 2006: Climate impacts of the Atlantic multidecadal oscillation. *Geophys. Res. Lett.*, **33**, L17706, doi:10.1029/2006GL026242.
- Kossin, J. P., and D. J. Vimont, 2007: A more general framework for understanding Atlantic hurricane variability and trends. *Bull. Amer. Meteor. Soc.*, **88**, 1767–1781.
- Latif, M., N. Keenlyside, and J. Bader, 2007: Tropical sea surface temperature, vertical wind shear, and hurricane development. *Geophys. Res. Lett.*, **34**, L01710, doi:10.1029/2006GL027969.
- Leloup, J., and A. C. Clement, 2009: Why is there a minimum in projected warming in the tropical North Atlantic Ocean? *Geophys. Res. Lett.*, **36**, L14802, doi:10.1029/2009GL038609.
- Saunders, M. A., and A. S. Lea, 2008: Large contribution of sea surface warming to recent increase in Atlantic hurricane activity. *Nature*, **451**, 557–560.
- Swanson, K. L., 2008: Nonlocality of Atlantic tropical cyclone intensities. *Geochem. Geophys. Geosyst.*, **9**, Q04V01, doi:10.1029/2007GC001844.
- Timmermann, A., and Coauthors, 2007: The influence of a weakening of the Atlantic meridional overturning circulation on ENSO. *J. Climate*, **20**, 4899–4919.
- Ting, M., Y. Kushnir, R. Seager, and C. Li, 2009: Forced and internal twentieth-century SST trends in the North Atlantic. *J. Climate*, **22**, 1469–1481.
- Vecchi, G. A., and B. J. Soden, 2007a: Effect of remote sea surface temperature change on tropical cyclone potential intensity. *Nature*, **450**, 1066–1070, doi:10.1038/nature06423.
- , and —, 2007b: Global warming and the weakening of the tropical circulation. *J. Climate*, **20**, 4316–4340.
- , and —, 2007c: Increased tropical Atlantic wind shear in model projections of global warming. *Geophys. Res. Lett.*, **34**, L08702, doi:10.1029/2006GL028905.
- , K. L. Swanson, and B. J. Soden, 2008: Whither hurricane activity? *Science*, **322**, 687–689, doi:10.1126/science.1164396.
- Vimont, D. J., and J. P. Kossin, 2007: The Atlantic meridional mode and hurricane activity. *Geophys. Res. Lett.*, **34**, L07709, doi:10.1029/2007GL029683.
- Wang, C., and S.-K. Lee, 2008: Global warming and United States landfalling hurricanes. *Geophys. Res. Lett.*, **35**, L02708, doi:10.1029/2007GL032396.
- , D. B. Enfield, S.-K. Lee, and C. W. Landsea, 2006: Influences of Atlantic warm pool on Western Hemisphere summer rainfall and Atlantic hurricanes. *J. Climate*, **19**, 3011–3028.
- , S.-K. Lee, and D. B. Enfield, 2008: Atlantic warm pool acting as a link between Atlantic multidecadal oscillation and Atlantic tropical cyclone activity. *Geochem. Geophys. Geosyst.*, **9**, Q05V03, doi:10.1029/2007GC001809.
- Xie, S.-P., C. Deser, G. A. Vecchi, J. Ma, H. Teng, and A. T. Wittenberg, 2010: Global warming pattern formation: Sea surface temperature and rainfall. *J. Climate*, **23**, 966–986.
- Zhang, R., 2007: Anticorrelated multidecadal variations between surface and subsurface tropical North Atlantic. *Geophys. Res. Lett.*, **34**, L12713, doi:10.1029/2007GL030225.
- , and T. L. Delworth, 2005: Simulated tropical response to a substantial weakening of the Atlantic thermohaline circulation. *J. Climate*, **18**, 1853–1860.
- , and —, 2006: Impact of Atlantic multidecadal oscillations on India/Sahel rainfall and Atlantic hurricanes. *Geophys. Res. Lett.*, **33**, L17712, doi:10.1029/2006GL026267.